UCRL-CONF-203633

LAWRENCE
LIVERMORE
NATIONAL
LABORATORY

Static and Time-Resolved 10-1000 keV X-Ray Imaging Detector

O.L. Landen, P.M. Bell, J.W. McDonald, H.-S. Park, F. Weber, J.D. Moody, M.E. Lowry, R.E. Stewart

April 16, 2004

15th Topical Conference on High Temperature Plasma Diagnostic, April 19-22, 2004, San Diego, CA

This document was prepared as an account of work sponsored by an agency of the United States Government. Neither the United States Government nor the University of California nor any of their employees, makes any warranty, express or implied, or assumes any legal liability or responsibility for the accuracy, completeness, or usefulness of any information, apparatus, product, or process disclosed, or represents that its use would not infringe privately owned rights. Reference herein to any specific commercial product, process, or service by trade name, trademark, manufacturer, or otherwise, does not necessarily constitute or imply its endorsement, recommendation, or favoring by the United States Government or the University of California. The views and opinions of authors expressed herein do not necessarily state or reflect those of the United States Government or the University of California, and shall not be used for advertising or product endorsement purposes.

Static and Time-Resolved 10-1000 keV X-Ray Imaging Detector Options for NIF*

O.L. Landen, P. M. Bell, J.W. McDonald, H.-S. Park, F. Weber, J. D. Moody, M.E. Lowry, R.E. Stewart

Lawrence Livermore National Laboratory, Livermore, CA USA 94551-0808

Abstract

High energy (> 10 keV) x-ray self-emission imaging and radiography will be essential components of many NIF High Energy Density Physics experiments. In preparation for such experiments, we have evaluated the pros and cons of various static (x-ray film, bare CCD, and scintillator + CCD) and time-resolved (streaked and gated) 10-1000 keV detectors.

*This work was performed under the auspices of U.S. Department of Energy by the University of California Lawrence Livermore National Laboratory under Contract No. W-7405-Eng-48.

Static Cameras

We begin by stipulating that a statistically acceptable x-ray image exposure should be at least 1000 photons detected per typical 10 x 10 μm NIF object resolution element. This requirement links the minimum *detected* image photon fluence I with the image magnification M via:

$$I\ (\text{photons}/\mu m^2) = 1000/(10M)^2 = 10/M^2 \qquad (1)$$

For AgBr-based x-ray film, the upper limit on detectable photon fluence based on a maximum film optical density of 5 [1,2] is $I_{max} \approx 30/E(\text{keV})$ ph/μm^2 over the range E = 10 and 100 keV photons. For a typical 10x10 μm pixel x-ray CCD with a full well capacity of 100,000 electrons / pixel and 1000E/3.7 e-h pairs formed per detected photon of energy E in keV, I_{max} = 3.7/E ph/μm^2 to avoid saturation [3]. For a scintillator coated optical CCD with same pixel size and full well capacity and including an x-ray to scintillator energy conversion efficiency η leads to $I_{max} = 3.7/\eta E$ ph/μm^2. Substituting into Eq. (1) yields minimum workable magnifications of M_{min} = $0.57\sqrt{E}$, $1.6\sqrt{E}$, $1.6\sqrt{(\eta E)}$, respectively. A second constraint on minimum magnification is that one must operate at < I_{max} fluence to provide some

single-shot dynamic range. The dynamic ranges DR, when defined as I_{max}/I and substituting for I using Eq. (1), are DR = $3M^2/E$, $0.37M^2/E$, $0.37M^2/\eta E$ respectively. A third constraint on the minimum magnification is set by the image plane resolution size being at least 2x the detector spatial resolution. For imaging between E = 10 - 100 keV, this approximately sets $M_{min} > 0.1E$ for film [1], M_{min} > max of 2, $.01E^{1.7}$ for Si-based CCDs, and $M_{min} > 0.2E$ [4 - 6] for high Z scintillator coated CCDs with thickness optimized for x-ray photon energy. A constraint on the maximum magnification is set by the maximum reasonable detector size. Setting the maximum detector size at 10 x 10 cm per frame and invoking a field-of-view of 10^4 resolution elements leads to a maximum magnification of 100x for 10 μm object resolution.

We can now compare the detector noise-limited SNR per resolution element (which can be expressed as a function of magnification via Eq. (1)) with the stipulated SNR per resolution element as set by photon statistics, i.e. SNR = $\sqrt{1000} \approx 30$. An acceptable detector must hence have a noise-limited SNR > 30.

For x-ray film, the sources of noise are fog noise and associated grain noise on the signal F. Typical fog noise is 300 developed grains/mm^2 [7], equivalent to 300 ph/mm^2 detected. The fog noise over a 10M μm image

resolution element is hence = 0.3/10M ph/μm^2. The grain noise has been shown to be nearly proportional to the signal (contrary to the $\sqrt{F}$ scaling for usual Poisson statistics) over a wide range of signal levels [8]. For DEF film, grain noise is measured at 10% of F averaged over 60 by 60 μm pixels. The grain noise over a resolution element is hence (0.1F)(60/10M) = $6/M^3$ ph/μm^2 after substituting for F using Eq. (1). The SNRs = F/Noise are hence given by 330/M, and 1.7M. for fog and grain noise, respectively.

For CCDs, the sources of noise are dark noise, read noise and Fano noise [9]. The sum of dark and read noise is typically 10 electrons / CCD pixel. Since a resolution element encompasses M^2 pixels in current case of object resolution = pixel size, the SNR as limited by dark and read noise = $(1000E/3.7)/(10\sqrt{M^2}) = 27E/M$.

The Fano noise is the fluctuation in the number of electron-hole pairs created per detected photon from a monochromatic source. This limits the energy resolution for CCDs in proportional counting mode, but also creates a fluctuation in the signal from resolution element to resolution element even for uniform exposure. The Poissonian Fano noise expressed as a fraction of the signal is typically $1.5/\sqrt{1000E}$ [9]. Hence the SNR averaged over a

resolution element containing 1000 x-ray photons detected = $\sqrt{(1000)}/(1.5/\sqrt{1000E})$.

For scintillator-coated CCDs, the sources of noise are dark noise, read noise and scintillator statistics noise [10]. Assuming a typical $\eta = 10\%$ [4], the SNR as limited by dark and read noise follows from before as $27\eta E/M = 2.7E/M$.

The scintillator statistical noise is the fluctuation in the number of optical photons created per detected photon from a monochromatic source. The Poissonian scintillator noise expressed as a fraction of the number of optical photons created per x-ray photon detected at <100 keV x-ray energies is given by $1/\sqrt{(1000\eta E/4)}$ assuming a typical 4 eV single quanta scintillation energy [10]. Ignoring the additional small inefficiency in CCD optical detection ($\approx 50\%$), the scintillator SNR averaged over a resolution element experiencing 1000 x-ray photons detected is then $\sqrt{1000}/(1/\sqrt{1000(\eta E/4)}) = 160\sqrt{E}$.

The various SNR limits are plotted in Figure 1 vs. image magnification for a photon energy of 37 keV. Also plotted on the abscissa are the dynamic

ranges. For film, the fog and grain noise have been added in quadrature. The open area below magnification 100 and above SNR = 30 represents the parameter space acceptable for experiments as discussed earlier. We note that the film fails to connect with this parameter space due to insufficient SNR as limited by fog and grain noise. The SNRs of the CCD and scintillator-CCD combination are limited by Fano and scintillator statistical noise rather than CCD electronic noise over the acceptable magnification range, but well above the required SNR as set by ensuring adequate x-ray photon statistics. We also note that the dynamic range of the scintillator coated CCD is 10x better than the uncoated CCD due to the beneficial inefficiency in the scintillator energy conversion.

Finally, it should be noted that while the film and CCD SNR curves on Fig. 1 will change slightly with photon energy, the same comparative conclusions will hold over the full range of photon energies between 10 and 100 keV. Furthermore, to consider a different object resolution s with the same number of photons per resolution element, one simply scales the magnification abscissa of Figure 1 by 1/s.

A further advantage of scintillator-coated CCDs is their high quantum efficiency (Q.E.). For example, a 150 μm-thick CsI scintillator maintaining

adequate spatial resolution [11] has Q.E. > 30% at energies up to 70 keV. For AgBr-based x-ray film such as DEF (26 μm-thick total emulsion)[2], Q.E. drops from 40% to 10% to < 1% as the photon energy is increased from 10 to 40 to 100 keV. For thick "deep-depletion" Si-based CCDs, Q.E. is comparable to film up to 25 keV and 2x worse between 25 and 50 keV. The main advantage of higher Q.E. is lower brightness requirements on the x-ray source and/or lower collection efficiency requirements on imaging optics.

Summarizing, the high Z scintillator coated CCD appears to provide the best combination of quantum efficiency, signal-to-noise and dynamic range at NIF-relevant imaging magnifications of 30-100x for time-integrated detection of 10-100 keV images. Film is not recommended. In the future, it will be instructive to compare the utility on NIF of other current and proposed detectors (e.g. time-integrating imaging plates and time-resolved detectors) using Figs. 1 and 2 as Figures-of-Merit.

Streak Cameras

We extend the calculation of the Q.E. of streak camera photocathodes, to > 10 keV by assuming as previously [12,13] that an x-ray photon of energy E with mean-free-path λ_X interacts with a photocathode by ejecting primary

photoelectrons and Auger electrons of total energy $E_P \approx E$. These primary electrons inelastically scatter over an escape depth λ_P continuously depositing a fraction f of their energy in the form of secondary electrons of energy E_S and escape depth ($\approx$ 1/2 range) λ_S [14]. Those secondary electrons that escape from the backside of the photocathode form the streak camera signal. With these definitions, the number of secondary electrons Y_S escaping per incident photon is the product of the fraction of incident photons absorbed over the quadrature sum λ of primary and secondary electron escape depths, the number of secondary electrons produced per photon absorbed, and the ratio of the secondary escape depth to the quadrature sum of primary and secondary electron escape depths:

$$Y_S = (\lambda/\lambda_X) \times f(E_P/E_S) \times (\lambda_S/\lambda) \qquad (2)$$

Eq. (2) assumes the photocathode thickness d satisfies the condition $\lambda < d < \lambda_X$, and simplifies to the λ and λ_P-independent formula presented in Ref. [13] for E < 10 keV. However, if $\lambda_P > d$ as can happen at higher photon energies, then the first λ term in Eq. (2) should be replaced by d. The first term is the maximum photocathode quantum efficiency ($Q.E._{MAX}$ = min. $(d/\lambda_X, \lambda/\lambda_X)$) possible. The product of the last two terms is the number N_S of

secondary electrons detected per photon *absorbed* within a λ escape depth of the back surface of the photocathode. Hence, we can rewrite Eq. (2) as Y_S = $Q.E._{MAX}$ x N_S.

Consider a CsI photocathode illuminated at E = 9 keV: $Y_S = 0.4$ for d = 102 nm, $\lambda_s = 25$ nm, $E_S = 1$ eV [13], $\lambda_P = 100$ nm [14] and $\lambda_X = 12.5$ µm. Hence the Q.E. $\approx \lambda_P/\lambda_X \approx 1\%$ since $d \geq \lambda$ and $N_S = 0.4/0.01 = 40 > 1$ satisfied. Furthermore, since Ref. [13] showed that E_S and λ_S are independent of E for a given photocathode, and that Y_S follows E_P/λ_X, then by inspection of Eq. (2), f is also a constant for a given photocathode, ≈ 0.02 for CsI.

When $N_S \approx f(E_P/E_S)(\lambda_S/\lambda_P)$ (for $\lambda_P > \lambda_S$) falls below 1 at other photon energies or for other photocathodes, Q.E is reduced by a factor $N_S < 1$ and is then identically equal to Y_S. Since $\lambda_P \sim E_P^{1.4}$, N_S will fall as $E_P^{-0.4} \approx E^{-0.4}$ far from edges. N_S is also smaller for smaller values of f (less energy deposited into secondaries) and shorter values of λ_S (typical of metals such as Au).

Figure 2 shows the predicted Q.E. vs incident photon energy for an optimized CsI transmission photocathode ($\lambda_P \leq d << \lambda_X$), which varies as expected as $\lambda_P/\lambda_X \approx E^{1.4}/E^{2.6} \approx E^{-1.2}$ well above edges. By comparison is

shown the predicted Q.E. for the cases of either $d < \lambda_P$ or assuming all secondaries are born at the photon absorption point, which drops faster as $1/\lambda_X \approx E^{-2.6}$. Existing secondary yield data [15] over the range E = 10 - 50 keV for a 100 nm-thickness ($< \lambda_P$) CsI photocathode follow a spectral sensitivity scaling in between these limits, so more research is recommended. In any case, even the optimized curve in Fig. 2 leaves room to develop improved quantum efficiency x-ray streak cameras for NIF, either extending the structured "fluffy" photocathodes to higher E or developing advanced CMOS or photonics based detectors [16].

Framing Cameras

Overplotted for comparison on Figure 2 is the Q.E. for standard 500-µm-thick microchannel plates used in x-ray framing cameras at 8° bias angle [17]. The MCP Q.E. is significantly larger than for streak cameras at high E because neighboring pore walls of thickness d act as multiple photocathodes when penetrated by > 10 keV x-rays even at grazing angles $\alpha \approx 6\text{-}8°$ (□□□> 30 µm > $d/\sin\alpha$ for E > 10 keV) □18□ The peaks at 20 and 100 keV are due to the Pb L and K edges in the leaded glass. Further improvements in Q.E. for E < 100 keV should be possible by coating the full length of the

pores with a high Z, high secondary electron range material such as CsI [19]. For E = 0.1 –1 MeV, Q.E.s reaching 1% have been demonstrated using thick Au planar photocathodes [20]. Non-MCP-based concepts now include fast gated CCD or CMOS detectors [21] and photonics based sensors [16].

References

[1] D. B. Brown, J. W. Criss, and L.S. Birks, J. Appl. Phys. **47** (1976) 3722; C. M. Dozier *et. al*., J. Appl. Phys. **47** (1976) 3732.

[2] P.D. Rockett, *et. al*., Appl. Opt. **24** (1985) 2536.

[3] J. Dunn, B. K. F. Young, and S. J. Shiromizu, Rev. Sci. Instrum. **66** (1995) 706.

[4] V. V. Nagarkar, *et. al*., IEEE Trans. Nucl. Sci. **46** (1999) 232.

[5] K. Sato, *et. al*., Rev. Sci. Instrum. **71** (2000) 4449.

[6] J. Wickersham, H-S. Park, *et. al*., Paper E46, this proceedings

[7] S. Gruner, Rev. Sci. Instrum. **60** (1989) 1545.

[8] J. D. Wiedwald, *et. al*., Proc. SPIE **1346** (1990) 200.

[9] A. Owens, *et. al.,* Proc. SPIE **4784** (2002) 244.

[10] C. W. E. van Eijk, Nuc. Instrum. Meth. A**471** (2002) 244.

[11] V. V. Nagarkar, *et. al*., IEEE Trans. Nucl. Sci. **45** (1998) 492.

[12] B.L. Henke, J.A. Smith and D.T. Attwood, J. Appl. Phys. **48** (1977) 1852.

[13] B.L. Henke, J.P. Knauer and K. Premaratne, J. Appl. Phys. **52** (1981) 1509.

[14] A. Gibrekhterman, A. Akkerman, A. Breskin, and R. Chechik, J. Appl. Phys. **74** (1993) 7506; A. Gibrekhterman, *et. al*., J. Appl. Phys. **76** (1994) 1676.

[15] T. Hara, *et. al*., Rev. Sci. Instrum. **71** (2000) 3624.

[16] M.E. Lowry, C.V. Bennett, *et. al*., SPIE Vol. 5194.

[17] J.E. Bateman, Nuc. Instrum. Meth. **144** (1977) 537;

[18] O.L. Landen, *et al*., Rev Sci Instrum. **72** (2001) 709; P.M. Shikaliev, Rev Sci Instrum. **68** (1997) 3676.

[19] G. Power and P. Bell, Proc. SPIE **981** (1988) 166.

[20] J. Veaux, *et. al*., Rev. Sci. Instrum., **62** (1991) 1562.

[21] R.K. Reich, *et. al*., Rev. Sci. Instrum. **74** (2003) 2027.

Figure Captions

Figure 1: Signal-to-noise contributions vs image magnification and dynamic range for detecting 1000 37 keV photons per 10 x 10 μm resolution element by film (dots), CCD (squares) and scintillator + CCD (triangles).

Figure 2: Predicted Q.E. for CsI transmission photocathode assuming λ_X > thickness ≥ $\lambda_{\square}$ □□□□, □□□□□□□□□thickness is constant and < λ_P but > λ_S (squares), and measured Q.E. (triangles) [17] for 400 μm-thick MCP.

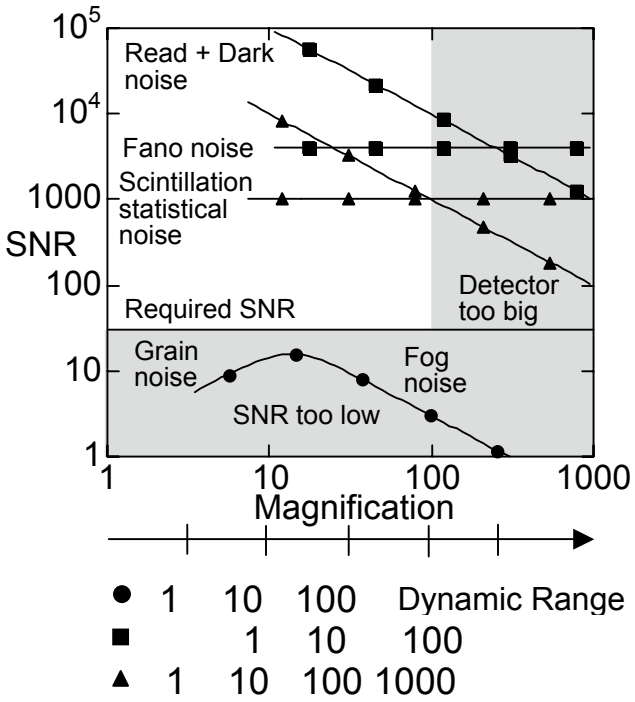

Figure 1, E40, Landen

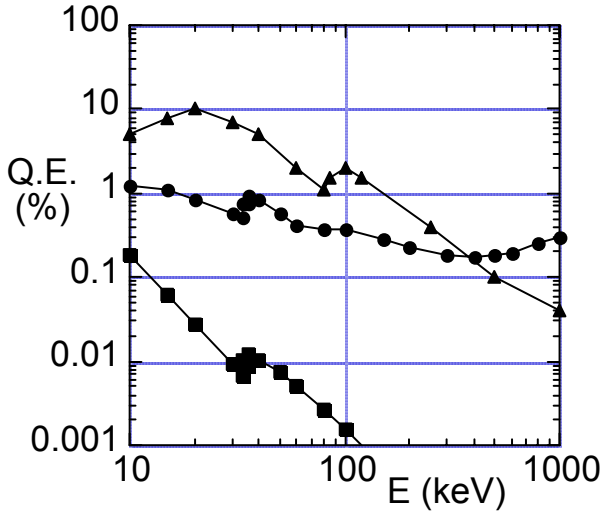

Figure 2, E40, Landen